CHAPTER 16

A Turbulent Flow Model For Breaking Waves

Nguyen The Duy[1], Tomoya Shibayama[2] and Akio Okayasu[2]

Abstract

This paper presents the formulation and solution of a numerical model for breaking waves on uniform sloping bottoms. The model is based on the two-dimensional vertical (2DV) Reynolds-averaged Navier-Stokes equations. The effect of breaker-generated turbulence is modeled by the Reynolds stress terms in the momentum equations, together with an eddy viscosity model. A transformation technique is utilized to solve numerically the governing equations in a variable grid system. At each time level of computation, it is possible to determine directly the following wave quantities for the surf zone: water surface elevation, pressure field and velocity field. The numerical results are verified with various cases of laboratory data.

1. Introduction

The breaking of waves results in the transformation of irrotational wave motion into turbulent rotational motion, which is characterized by vortex motion of various scales; and due to this turbulent motion, the wave energy transported from the offshore is dissipated throughout the surf zone. It has been known that turbulence generated by breaking waves has important effects on most processes within the surf zone such as wave transformation, diffusion of materials, etc. Therefore, in order to obtain a realistic and reasonable simulation of surf zone processes, it is necessary to include the effect of turbulence in the formulation of the wave equations. In addition, information on the vertical structure of wave variables such as wave pressure and water particle velocities is necessary to solve important problems of the nearshore area. For instance, the vertical profile of wave pressure can be applied to determine acting force used in the design of coastal structures, or the near-bottom velocity can be used as a boundary condition to determine the bed shear stress and to solve the flow inside the bottom boundary layer which, in turn, play an important role in the prediction of beach profile

---

[1]Dr. Eng., Dept. of Civil Eng., Ho Chi Minh City Univ. of Technology, 268 Ly Thuong Kiet, Q. 10, Ho Chi Minh City, Vietnam.
[2]Dr. Eng., Assoc. Prof., Dept. of Civil Eng., Yokohama National Univ., Hodogaya-ku, Yokohama 240, Japan.

change due to sediment transport. An useful and effective wave model, therefore, must be eapable of computing directly the vertieal distribution of wave variables.

Reeently, rapid development in the memory capacity and computational speed of personal eomputers makes it possible to solve the full 2DV Navier-Stokes equations for water waves. The solution of 2DV wave models may be one among preliminary steps to achieve a eomplete pieture of the modeling of eoastal hydrodynamies in a near future, when water waves can be simulated by solving the full three-dimensional Navier-Stokes equations.

Petit et al. (1994) eomputed breaking waves on a submerged bar by applying the Volume of Fluid method to solve the 2DV Navier-Stokes equations. Shibayama and Duy (1994) presented a 2DV model for waves propagating on sloping bottoms and verified it with laboratory data of non-breaking and breaking waves, however, they could not attain reasonable numerieal results for the veloeity field in the surf zone.

This paper presents a hydrodynamic model for breaking waves on uniform sloping bottoms, in which the effeet of breaker-generated turbulenee and the depth variation of the wave variables are included in the model.

2. Governing Equations

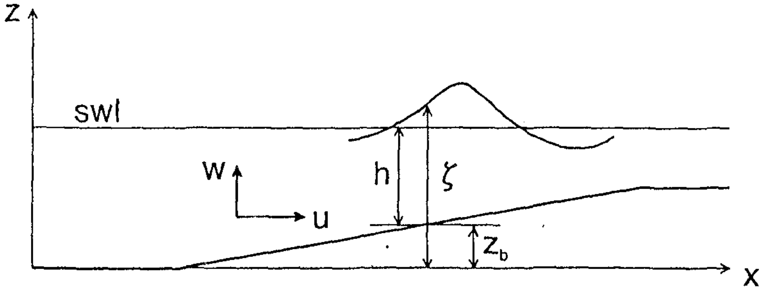

Figure 1: Definition sketeh of eoordinates system

For a free surface domain, the 2DV Reynolds-averaged Navier-Stokes equations are written as

$$\frac{\partial u}{\partial x}+\frac{\partial w}{\partial z}=0 \tag{1}$$

$$\frac{\partial u}{\partial t}+\frac{\partial (u^2)}{\partial x}+\frac{\partial (uw)}{\partial z}=-\frac{1}{\rho}\frac{\partial P}{\partial x}+M_x \tag{2}$$

$$\frac{\partial w}{\partial t}+\frac{\partial (uw)}{\partial x}+\frac{\partial (w^2)}{\partial z}=-g-\frac{1}{\rho}\frac{\partial P}{\partial z}+M_z \tag{3}$$

$$\frac{\partial \zeta}{\partial t}+\frac{\partial}{\partial x}\int_{z_b}^{\zeta} u\,dz=0 \tag{4}$$

where (u,w): Reynolds-averaged veloeity veetor; P: Reynolds-averaged pressure; ζ: water surface elevation; z_b: sea bottom elevation; g: gravity aeeeleration. The momentum transports due to fluctuating velocity components of turbulent motion (Reynolds stress terms), M_x and M_z, can be expressed as follows, by using eddy viscosity model

$$M_x = 2\frac{\partial}{\partial x}\left(\nu_T \frac{\partial u}{\partial x}\right) + \frac{\partial}{\partial z}\left[\nu_T\left(\frac{\partial u}{\partial z} + \frac{\partial w}{\partial x}\right)\right] \tag{5}$$

$$M_z = \frac{\partial}{\partial x}\left[\nu_T\left(\frac{\partial u}{\partial z} + \frac{\partial w}{\partial x}\right)\right] + 2\frac{\partial}{\partial z}\left(\nu_T \frac{\partial w}{\partial z}\right) \tag{6}$$

where ν_T is the eddy viscosity. In the above equations, since $\nu << \nu_T$, the diffusive terms due to molecular viscosity ν are neglected.

In the surf zone, the mean value (time-averaged over one wave period) of ν_T, $\overline{\nu}_T$, has been previously determined by fitting computed currents velocities to measured data. For instance, Longuet-Higgins (1970) simulated longshore currents by using

$$\overline{\nu}_T \approx 0.01 h\sqrt{gh} / s \tag{7}$$

where h is the mean water depth and s the beach slope.

On the other hand, in the modeling of cross-shore currents, Okayasu et al. (1988) applied a mean eddy viscosity in the form

$$\overline{\nu}_T = 0.3\sqrt{g(d_t + H)}\, s\, z' \tag{8}$$

in which d_t is the depth to wave trough, H the wave height and z' the vertical distance from the bottom, while Svendsen and Hansen (1988) suggested that

$$\overline{\nu}_T = (0.007 - 0.03) h\sqrt{gh} \tag{9}$$

Based on Eq. (9) and the Prandtl-Kolmogorov assumption, Shibayama and Duy (1994) derived approximately a time-varying eddy viscosity for the area outside the bottom boundary layer of the surf zone as follows

$$\nu_T = f_v \sqrt{gh}\,(\zeta - z_b) \tag{10}$$

In Eq. (10), f_v is a constant and was found to have an average value of 0.125 from the computations of breaking waves. Shibayama and Duy (1994) showed that the use of a fixed value of f_v for all computational cases can produce good agreements between computed and measured wave heights in the surf zone, however, simulated wave profiles and velocity field generally exhibit certain discrepancies compared to measured data, in particular for the near-breaking area. These discrepancies may be caused by the fact that the eddy viscosity commonly increases within certain distance from the breaking point, as shown by laboratory measurements of Okayasu et al. (1988). In order to take into account this effect in the simulation, the constant f_v is slightly modified to become

$$f_v = \begin{cases} 0.03 e^{h_b/h} & \text{if } h_b / h < 1.5 \\ 0.03 e^{1.5} & \text{if } h_b / h \geq 1.5 \end{cases} \tag{11}$$

where h is the still water depth, and h_b the breaking water depth. Eq. (11) expresses a variation range of f_v from a minimum value of 0.082 at the breaking point ($h_b / h = 1$) to a maximum value of 0.134.

Boundary Conditions:

- *Water surface boundary* $(z = \zeta)$:

The water surface is a moving boundary in the model. The position of this boundary must be determined at each time level with its own boundary conditions as follows.

For u, a zero shear stress condition is assumed at the water surface

$$\frac{\partial u}{\partial z} = 0 \tag{12}$$

For w, the kinematic boundary condition at a free surface is applied:

$$w = \frac{\partial \zeta}{\partial t} + u\frac{\partial \zeta}{\partial x} \tag{13}$$

and the boundary condition for P is

$$P = 0 \tag{14}$$

- *Bottom Boundary* $(z = z_b)$:

A non-slip condition is applied for w:

$$w = 0 \tag{15}$$

In the numerical mesh, the first grid point of u is not located at the bottom (Fig. 2) and therefore, a direct use of the non-slip condition is not necessary. Instead, the boundary condition of u is given implicitly in the form

$$u_{i+0.5,1} + u_{i+0.5,2} = 0 \tag{16}$$

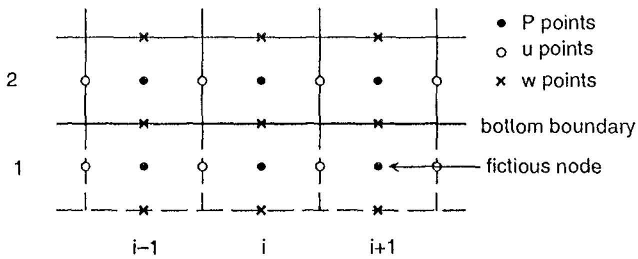

Figure 2: Bottom boundary

Using the continuity equation, Eq. (1), and the non-slip condition, a Neumann boundary condition for pressure is obtained from the z-momentum equation, Eq. (3):

$$\frac{\partial P}{\partial z} = \rho\left[-g + 2\nu_T \frac{\partial^2 w}{\partial z^2}\right] \tag{17}$$

- *Seaward Boundary* $(x = 0)$

The boundary conditions for ζ, u, w and P of incident wave are obtained by applying cnoidal wave theory or Stokes wave theory, depending on the calculated Ursell parameter, Ur, at the seaward boundary (Nishimura et al., 1977):

$$U_r = \frac{HL^2}{h^3} \begin{cases} \geq 25 & : \textit{cnoidal waves} \\ < 25 & : \textit{Stokes waves} \end{cases} \tag{18}$$

The reflected wave from the domain inside, if existing, will be treated to pass freely and undisturbed through the open seaward boundary. In the model, the actual water surface at each time level t is computed as the sum of the incident and reflected waves.

After determining the water surface elevation ζ (t), the other variables at the seaward boundary (u, w, P) can be determined approximately by using cnoidal or Stokes wave theory depending on the value of Ursell parameter.

- *Shoreline Boundary* $(x = x_{\max})$

For u, an absorbing boundary condition is applied at the shoreline boundary (Zienkiewicz and Taylor, 1991):

$$\frac{\partial u}{\partial t} + c\frac{\partial u}{\partial x} = 0 \tag{19}$$

where c is the wave celerity at the shoreline boundary. For outflow at the shoreline boundary, typical boundary condition for w is (Fletcher, 1991)

$$\frac{\partial w}{\partial x} = 0 \tag{20}$$

Assuming that the effect of viscosity in the region adjacent to the shoreline is negligible, a Neumann boundary condition for pressure P can be derived by using the x-momentum equation, Eq. (2), and the absorbing condition, Eq. (19). The resultant equation is

$$\frac{\partial P}{\partial x} = -\rho\left[(2u - c)\frac{\partial u}{\partial x} + \frac{\partial (uw)}{\partial z}\right] \tag{21}$$

- *Breaking Location* $(x = x_b)$

The breaking point is determined by Goda's breaking indices (1975):

$$\frac{H_b}{L_0} = A\left\{1 - \exp\left[-1.5\frac{\pi h_b}{L_0}\left(1 + 15s^{4/3}\right)\right]\right\} \tag{22}$$

where H_b: breaking wave height; L_0: deep water wave length; s: beach slope; and A is an empirical constant taken to be 0.17.

3. Numerical Formulation

In the physical domain, the upper surface is a moving boundary due to wave motion, and the sea bottom also changes in space,

$$\zeta = \zeta(x,t) \tag{23}$$

$$z_b = z_b(x) \tag{24}$$

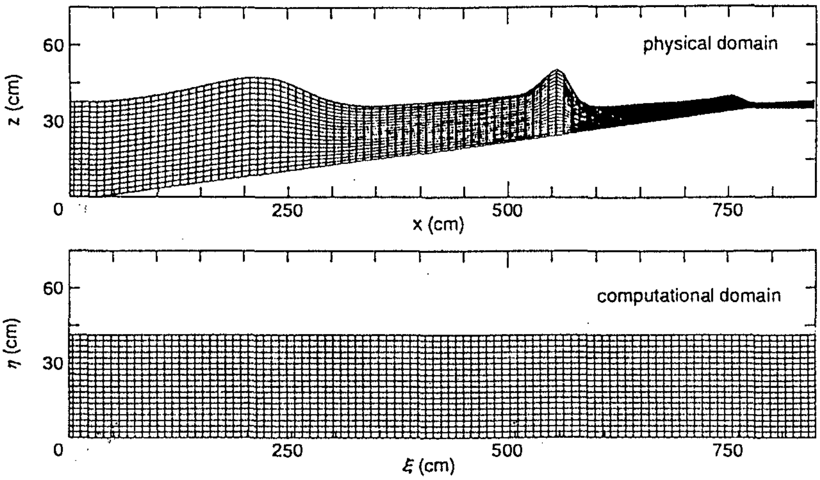

Figure 3: Physical and computational domain

The generated grid for numerical computation is thus also a moving system in space and time (Fig. 3). It is difficult to solve the governing equations numerically in this moving and curvilinear grid. Therefore, a coordinate transformation is carried out to map the moving grid to a fixed and linear one, in which the boundaries are parallel to the coordinate-axes (Fig. 3). The relationships between the physical domain (x, z, t) and the computational domain (ξ, η, τ) are expressed as follows

$$x = \xi \tag{25}$$

$$z = z_b + f(\eta^*)(\zeta - z_b) \tag{26}$$

$$t = \tau \tag{27}$$

where $\eta^* = \eta / \eta_m$ and η_m is the maximum value of η.

Depending on the form of the function $f(\eta^*)$, different types of numerical mesh can be generated for the physical domain (Fletcher, 1991). To obtain constant vertical mesh intervals in the physical domain, we choose

$$f(\eta^*) = \eta^* \tag{28}$$

The first deriatives of the velocity components, u and w, with respect to x, z, and t are expressed in terms of the new variables ξ, η, τ as follows:

$$\begin{bmatrix} \frac{\partial u}{\partial x} & \frac{\partial u}{\partial z} & \frac{\partial u}{\partial t} \\ \frac{\partial w}{\partial x} & \frac{\partial w}{\partial z} & \frac{\partial w}{\partial t} \end{bmatrix} = \begin{bmatrix} \frac{\partial u}{\partial \xi} & \frac{\partial u}{\partial \eta} & \frac{\partial u}{\partial \tau} \\ \frac{\partial w}{\partial \xi} & \frac{\partial w}{\partial \eta} & \frac{\partial w}{\partial \tau} \end{bmatrix} \begin{bmatrix} \frac{\partial \xi}{\partial x} & \frac{\partial \xi}{\partial z} & \frac{\partial \xi}{\partial t} \\ \frac{\partial \eta}{\partial x} & \frac{\partial \eta}{\partial z} & \frac{\partial \eta}{\partial t} \\ \frac{\partial \tau}{\partial x} & \frac{\partial \tau}{\partial z} & \frac{\partial \tau}{\partial t} \end{bmatrix} \tag{29}$$

where the Jacobian matrix J of the transformation is determined by using Eqs. (25) through (27)

$$J=\begin{bmatrix} \frac{\partial\xi}{\partial x} & \frac{\partial\xi}{\partial z} & \frac{\partial\xi}{\partial t} \\ \frac{\partial\eta}{\partial x} & \frac{\partial\eta}{\partial z} & \frac{\partial\eta}{\partial t} \\ \frac{\partial\tau}{\partial x} & \frac{\partial\tau}{\partial z} & \frac{\partial\tau}{\partial t} \end{bmatrix}=\begin{bmatrix} 1 & 0 & 0 \\ -\frac{\left[\eta_m z_{bx}+\eta\left(\zeta_x-z_{bx}\right)\right]}{\zeta-z_b} & \frac{\eta_m}{\zeta-z_b} & -\eta\frac{\zeta_t}{\zeta-z_b} \\ 0 & 0 & 1 \end{bmatrix} \tag{30}$$

where ζ_x and z_{bx} denote the derivatives of ζ and z_b with respect to x, respectively.

With the obtained Jacobian matrix J, at each time level the variable physical domain (x, z, t) can be transformed to the fixed computational domain (ξ,η,τ). The governing equations, Eqs. (1) through (4), in the computational domain are then given as:

$$\frac{\partial u}{\partial\xi}+\eta_x\frac{\partial u}{\partial\eta}+\eta_z\frac{\partial w}{\partial\eta}=0 \tag{31}$$

$$\frac{\partial u}{\partial\tau}+\eta_t\frac{\partial u}{\partial\eta}+\frac{\partial\left(u^2\right)}{\partial\xi}+\eta_x\frac{\partial\left(u^2\right)}{\partial\eta}+\eta_z\frac{\partial(uw)}{\partial\eta}=-\frac{1}{\rho}\left(\frac{\partial P}{\partial\xi}+\eta_x\frac{\partial P}{\partial\eta}\right)+M_\xi \tag{32}$$

$$\frac{\partial w}{\partial\tau}+\eta_t\frac{\partial w}{\partial\eta}+\frac{\partial(uw)}{\partial\xi}+\eta_x\frac{\partial(uw)}{\partial\eta}+\eta_z\frac{\partial\left(w^2\right)}{\partial\eta}=-g-\frac{\eta_z}{\rho}\frac{\partial P}{\partial\eta}+M_\eta \tag{33}$$

$$\frac{\partial\zeta}{\partial t}+\frac{\partial}{\partial x}\int_{z_b}^{\zeta}u\,dz=0 \tag{34}$$

where

$$\begin{aligned} M_\xi &= 2\left(\frac{\partial v_T}{\partial\xi}+\eta_x\frac{\partial v_T}{\partial\eta}\right)\left(\frac{\partial u}{\partial\xi}+\eta_x\frac{\partial u}{\partial\eta}\right)+\eta_z^2\left(\frac{\partial v_T}{\partial\eta}\frac{\partial u}{\partial\eta}+v_T\frac{\partial^2 u}{\partial\eta^2}\right) \\ &\quad +2v_T\left[\frac{\partial^2 u}{\partial\xi^2}+\eta_x^2\frac{\partial^2 u}{\partial\eta^2}+2\eta_x\frac{\partial^2 u}{\partial\xi\partial\eta}+\frac{\partial u}{\partial\eta}\left(\frac{\partial\eta_x}{\partial\xi}+\eta_x\frac{\partial\eta_x}{\partial\eta}\right)\right] \end{aligned} \tag{35}$$

$$\begin{aligned} M_\xi &= \left(\frac{\partial v_T}{\partial\xi}+\eta_x\frac{\partial v_T}{\partial\eta}\right)\left(\frac{\partial w}{\partial\xi}+\eta_x\frac{\partial w}{\partial\eta}\right)+2\eta_z^2\left(\frac{\partial v_T}{\partial\eta}\frac{\partial w}{\partial\eta}+v_T\frac{\partial^2 w}{\partial\eta^2}\right) \\ &\quad +v_T\left[\frac{\partial^2 w}{\partial\xi^2}+\eta_x^2\frac{\partial^2 w}{\partial\eta^2}+2\eta_x\frac{\partial^2 w}{\partial\xi\partial\eta}+\frac{\partial w}{\partial\eta}\left(\frac{\partial\eta_x}{\partial\xi}+\eta_x\frac{\partial\eta_x}{\partial\eta}\right)\right] \end{aligned} \tag{36}$$

The boundary conditions are also transformed to the computational domain in the similar way. The transformed equations and corresponding boundary conditions can be solved numerically by the finite difference method. The numerical computation is carried out on a staggered grid. In this staggered grid, P is defined at the centre of each cell and u, w are defined at the cell faces. In discretizing Eqs. (31), (32), (33), (34), finite difference expressions centered at grid point (i, j), ($i+0.5$, j), (i, $j+0.5$), and (i, j) are used, respectively. These allow all derivatives can be discretised in second-order accuracy with smallest number of involved grid points. The use of the staggered grid also permits coupling of the u, w and P solutions at adjacent grid points. This in turn prevents the appearance of oscillatory solutions, particularly for P, that can occur if centred differences are used to discretise all derivatives on a non-staggered grid.

A semi-implicit scheme is utilized to solve numerically the discretized forms of Eqs. (31) through (34). At each time step, a main set of linear equations for pressure is solved for the total number of grid points and subordinate sets of linear equations for velocities are solved along the boundaries. The result of pressure distribution is then used to compute the velocity field. For the water surface, two computational steps are necessary to determine this moving boundary at each time step as follows.

(i) At the beginning of a time step $n+1$, an approximate solution for the water surface is obtained by applying an explicit finite difference scheme for Eq. (31), using velocity profiles at the previous time step n. The water surface obtained is then used to evaluate the elements of the Jacobian matrix, and therefore the transformed equations (31) through (34) can be solved in the computational domain.

(ii) At the end of the time step $n+1$, after finishing the velocity computation, an improvement on the water surface computation is achieved by applying the Crank-Nicolson scheme for Eq. (31), using velocity profiles at both time steps n and $n+1$.

4. Numerical results

The total computational time required for the model to get the final results depends mainly on the number of grid points used in the mesh. Using a HP9000/720, it takes approximately 1 hour to complete one simulation for a mesh of 2000 grid points.

A typical illustration of the convergence and stability characteristic of the present model is presented in Fig. 4, which are the computed wave profiles at different sections in the surf zone. With the still water level (horizontal line) is set as the initial condition of the computation, it can be seen that after only about two waves coming from the offshore boundary, the computed wave profile at each section already converts to its final solution. This behavior indicates a rapid convergence characteristic of the model. After the convergence point, the stability of the solution can also be seen through the periodical results of the computed wave profiles.

A typical example of the numerical results of the hydrodynamic model are shown in Figs. 5 and 6. The model results are verified with the laboratory data obtained by Okayasu et al. (1988). In the figures, the variable X denotes horizontal distance from the shoreline of the still water, subscript "b" denotes the breaking point, and z' is the vertical elevation from the bottom.

Fig. 5 shows that the time history of water surface elevation follows an asymetric pattern: the rise of water surface occurs much faster than the fall one. In general, the model is capable of simulating the highly nonlinear and asymmetric characteristics of wave profiles in the surf zone, as shown through the comparisons with measured data. However, as a common result, large discrepancies between the computed and measured wave profiles are observed at sections close to the shoreline. These discrepancies may have been caused by the effect of the shoreline boundary. The verifications also show that the present model is capable of

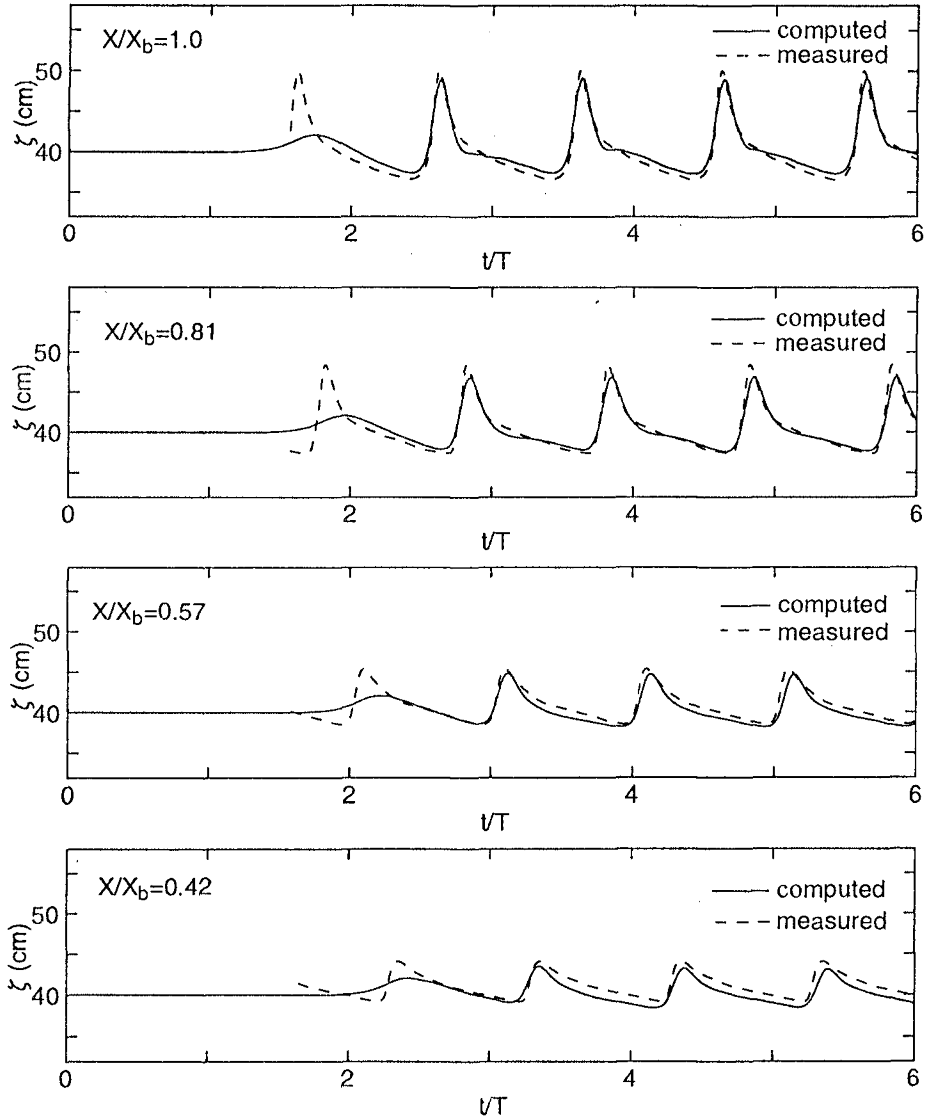

Figure 4: Convergence and stability characteristics of the present model, illustrated through the time series of equi-phase mean water surface elevation ($H_0 = 8.5cm$, $T=2s$, $h_0 = 40cm$, $s=1/20$).

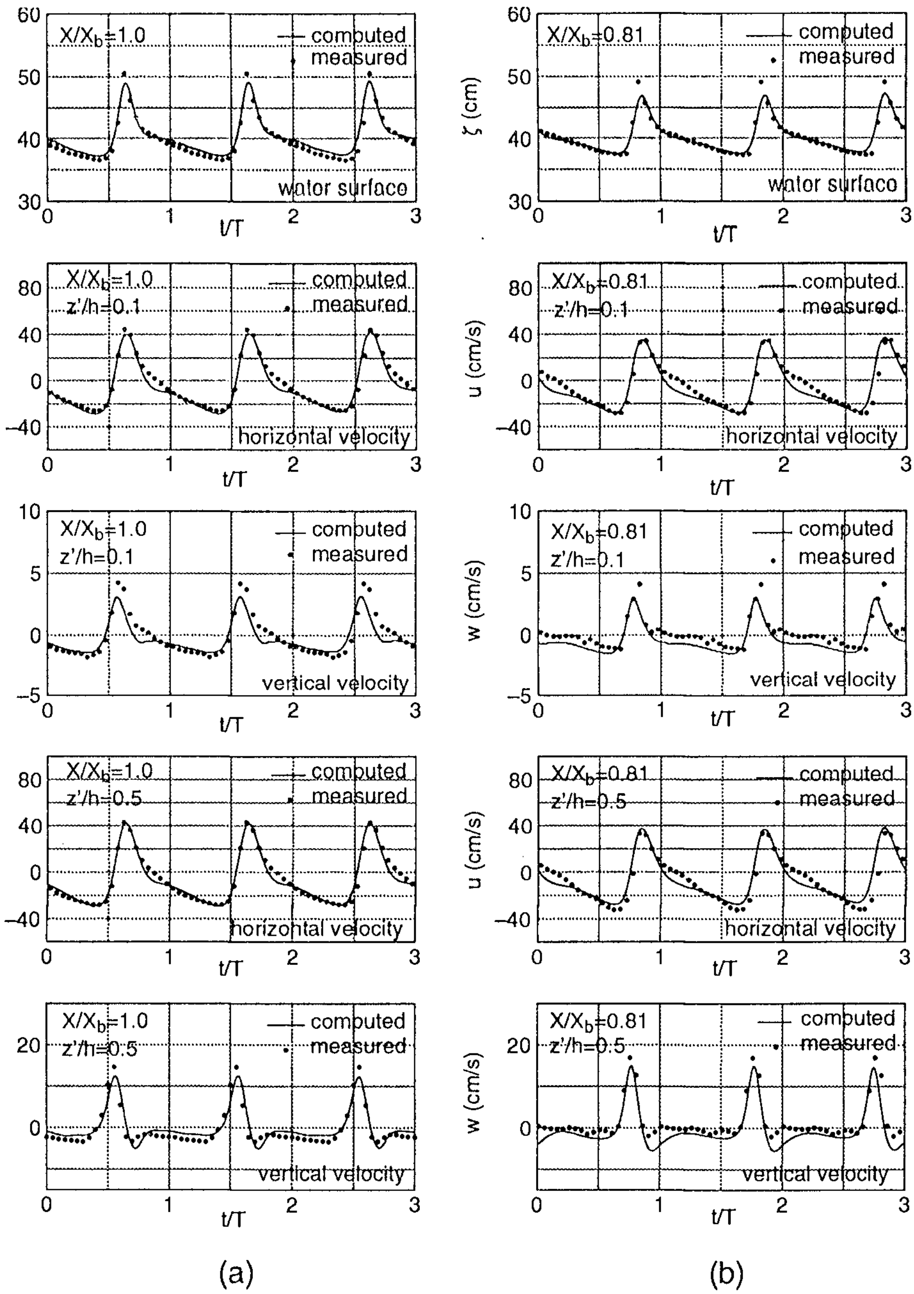
X/Xb=1.0
computed
measured
water surface
t/T
horizontal velocity
vertical velocity
z'/h=0.1
z'/h=0.5
X/Xb=0.81
ζ (cm)
u (cm/s)
w (cm/s)
(a)
(b)

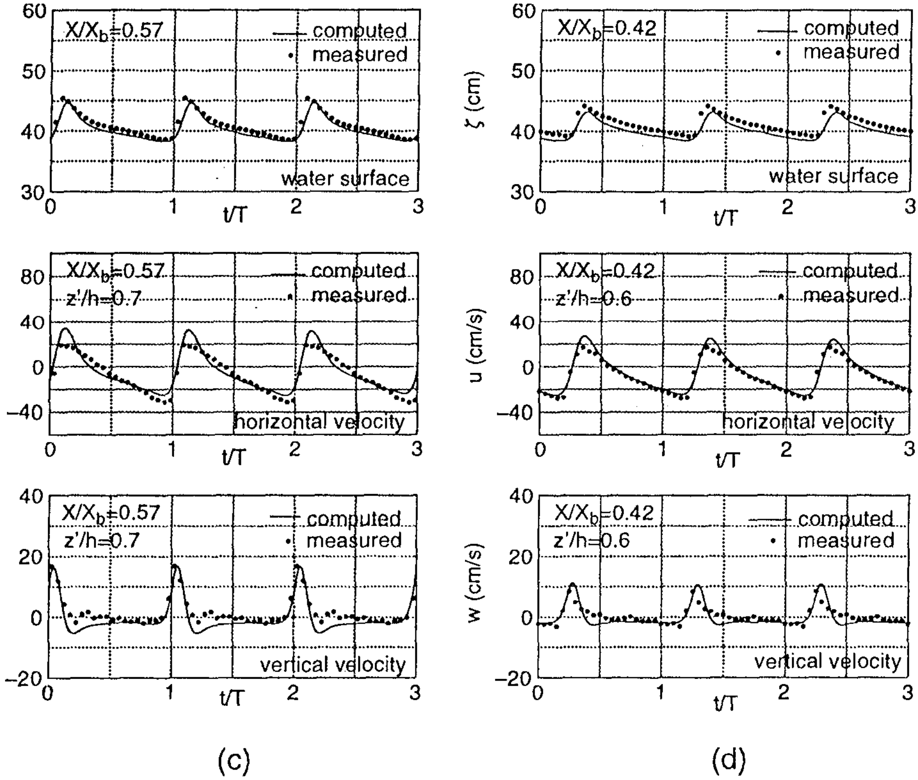

Figure 5: Time histories of water surface elevation ζ, horizontal velocity u and vertical velocity w at different sections and elevations in the surf zone (H_0 = 8.5*cm*, *T*=2*s*, h_0 = 40*cm*, *s*=*1/20*).

simulating the deformation of the velocity profiles as the wave propagates shoreward and of producing the high nonlinearity and asymmetry of the velocity profiles in shallow water area (Fig. 5). Generally, reasonable agreements, both in magnitude and phase, are obtained between the computed velocities and the laboratory data. In the vicinity of the breaking point, however, the vertical velocity is somewhat underestimated by the model. And at sections close to the shoreline, the model overestimates the peak value of the horizontal velocity. The simulation results also show that, in the surf zone, the vertical velocity magnitude at most elevations is considerable compared to the horizontal velocity magnitude and therefore cannot be neglected in the computation as is done in most existing wave models.

The equi-phase mean velocity vectors in the measured area of the surf zone are plotted in Fig. 6, for different phases in one wave period. A fairly good agreement in the direction and the magnitude between the computed and measured velocity vectors can be observed, but there exist small discrepancies in the near-bottom area. In bottom area, the simulated velocity vectors exhibit smaller values than the measured ones. Small discrepancies between the computed and measured velocity vectors can also be seen in the vicinity of the shoreline. This may be due to the fact that the real shoreline boundary has not yet been simulated perfectly in the model and may cause certain effects on the computed velocity field.

5. Conclusions

- In the present model, the hydrodynamics of breaking waves in the surf zone was investigated based on the governing equations of turbulent flow: the Reynolds-averaged Navier-Stokes equations. The effect of breaker-generated turbulence was included in the model and the vertical distribution of wave variables (P, u, w) can be computed directly by the model. The numerical results agree reasonably well with laboratory data of 2DV velocity field and water surface elevation in the surf zone.
- A time-dependent eddy viscosity was introduced in the present study to solve the 2DV Reynolds-averaged Navier-Stokes equations. The derived eddy viscosity has been verified to be applicable in the modeling of breaking waves. However, this is only one of the possible alternatives in determining the eddy viscosity. The present model may be tested with other solutions of the eddy viscosity in order to seek for possible improvements of the simulation results.
- In the model, it is possible to determine only the vertical distribution of horizontal velocity from the water surface to the first grid point above the bottom. The horizontal velocity profile below this grid point, which is affected by the bottom boundary layer (BBL), has not yet been computed by the model. The inclusion of the effect of the BBL requires a very fine mesh interval, whose order is about $0.1mm$, in order to model the large velocity gradient in the near-bottom area. However, at present, a 2DV hydrodynamic simulation of the entire surf zone, in which the BBL is included, is still not economical in sense of the CPU time required.
- Disagreements between the numerical results and the laboratory data commonly occur in the area close to the shoreline. As already mentioned, these poor agreements may have been caused by the effect of the shoreline boundary. Due to certain technical problems encountered in the formulation of a 2DV model, some assumptions have been made to simplify the implementation of the shoreline boundary conditions such as the absorbing condition for u, the uniform condition for w. These assumptions may not reflect properly the realistic phenomena at the shoreline boundary. Therefore, a more reasonable implementation of the shoreline boundary conditions is necessary to obtain better simulation results in the area close to the shoreline.

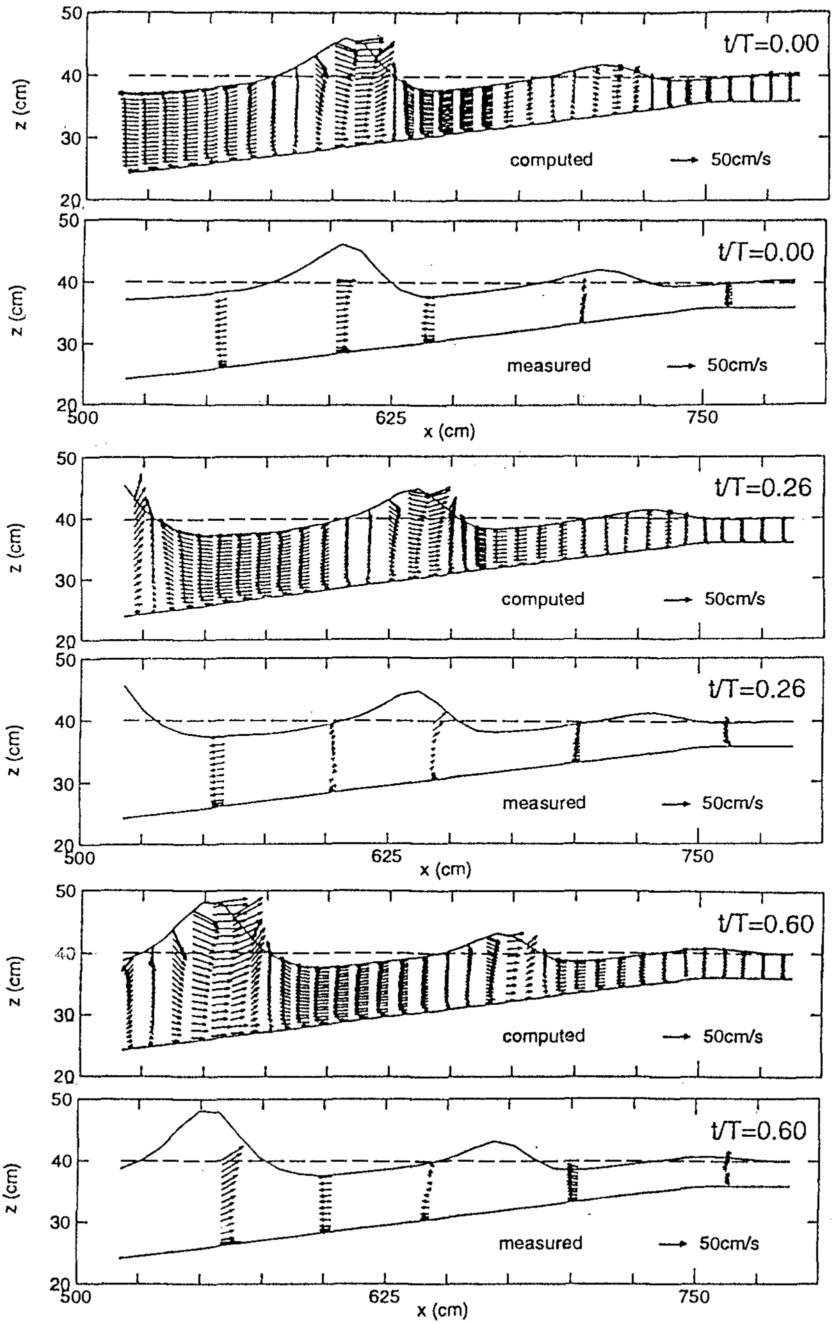

Figure 6: Comparison of equi-phase mean velocity vectors in the surf zone (H_0 = 9.87cm , T=$1.17s$, h_0 = 40cm, s=$1/20$).

References

Fletcher, C.A.J. (1991). *Computational Techniques for Fluid Dynamics*. Vol. 1,2, 2nd edition, Springer-Verlag, Berlin Heidelberg, 299-328.

Goda, Y. (1975). Deformation of irregular waves due to depth-controlled wave breaking. *Report of the Port and Harbour Tech. Res. Inst., 14-(3)*.

Longuet-Higgins, M.S. (1970). Longshore currents generated by obliquely incident sea waves. *J. of Geophys. Res., 75*, 6790-6801.

Nishimura, H., M. Isobe, and K. Horikawa (1977). Higher order solutions of the Stokes and the cnoidal waves. *J. Fac. Eng., Univ. of Tokyo, B-34, No. 2*, 267-293.

Okayasu, A., T. Shibayama, and K. Horikawa (1988). Vertical variation of undertow in the surf zone. *Proc. 21st ICCE, ASCE*, 478-491.

Petit, H.A.H., P. Tonjes, M.R.A. van Gent, and P. van den Bosch (1994). Numerical simulation and validation of plunging breakers using a 2D Navier-Stokes model. *Proc. 23rd ICCE, ASCE*, 511-524.

Shibayama, T. and N.T. Duy (1994). A 2D vertical model for wave and current in the surf zone based on the turbulent flow equations. *Coastal Eng. in Japan, JSCE, 37-(1)*, 41-65.

Svendsen, I.A., and J.B. Hansen (1988). Cross-shore currents in surf zone modeling. *Coastal Eng., Elsevier*, 12, 23-42.

Zienkiewicz, O.C. and R.L. Taylor (1991). *The Finite Element Method.* Vol. II, McGraw-Hill, 4th edition, 807 pages.